

Effects of nano aluminum nitride on the microstructure and mechanical properties of vitrified bond diamond tools

Kuan-Hong Lin^{a,*}, Yuo-Tern Tsai^b and Ke-Lun Wang^a

^aDepartment of Mechanical Engineering, Tunghan University, New Taipei City 222, Taiwan, ROC

^bDepartment of Mechanical Engineering, HungKuo Delin University of Technology, New Taipei City 236, Taiwan, ROC

This study investigated the effects of nano aluminum nitride (AlN) on the microstructure and mechanical properties of vitrified bond diamond tools. Raman spectra analysis indicated that added nano AlN helped to protect the diamond crystal structure during sintering. The diffraction peaks of diamond, AlN, Al₂O₃, and a few of SiO₂ crystal were observed in the X-ray diffraction analysis. However, a lower sintering temperature of 690 °C in this study decreased the formation of Al₂O₃ and α -SiO₂ phases. Scanning electron microscope images showed that addition of 10 vol% nano AlN into the specimen provided an appropriate wetting and bonding between the diamond grits and the matrix, thus producing the highest grinding ratio (24.1) of the tools and the best workpiece surface roughness. The added amount of nano AlN higher than 20 vol% would trigger gas eruption from the matrix during the sintering process, which produced a larger number of pores and caused the vitrified matrix expansion. The deteriorated microstructure decreased the mechanical properties of vitrified bond diamond tools.

Key words: Nano AlN, Vitrified bond diamond tool, Microstructure, Grinding ratio.

Introduction

The pores of different sizes can be easily introduced into the matrix structure; therefore vitrified bond diamond (VBD) tools generally have an outstanding capacity for the chips removal and heat dissipation. As a result, VBD tools possess an excellent grinding performance, and the workpieces that can maintain a preferred surface roughness [1-6]. However, the artificial diamonds usually contain some active metal components that can cause the diamonds to be catalyzed easily, and transformed from diamond structures into graphite during sintering process, consequently decreasing the mechanical properties of the VBD tools. Solutions aimed at addressing this phenomenon include the following: sintering at low temperatures, decreasing the isothermal holding duration, introducing a protective atmosphere, and the addition of elements that provide protection for the diamond grits [7-14].

However, sintering at low temperatures or decreasing the isothermal holding duration caused the insufficient bonding force between the diamond grit and the vitrified matrix, thus increasing the likelihood of the diamond grit being pulled off from the matrix when the given diamond is still sharp. Consequently, decreasing the grinding efficiency of the VBD tool and increasing the workpiece surface roughness [1-3, 15]. Previous

studies have indicated that the appropriate sintering parameters for the diamond/borosilicate glass composites are a sintering temperature of 710 °C and isothermal holding duration of 90 min [2, 3]. In this study, we hoped to realize whether the addition of nano aluminum nitride (nano AlN) to the specimen would allow for a reduction of the sintering temperature and isothermal holding duration, as well as promotion the grinding performance of VBD tools.

Previous studies have indicated that nano AlN has high surface energy; thus adding it into glass matrix can assist in reducing the sintering temperature required [12]. Researchers also noted that nano AlN sintered at 730 °C in the air becomes oxidized and decomposed into Al₂O₃ and gas, as well as result in the porosity increased in the matrix structure [11]. Those studies also found that when nano AlN is sintered at 730 °C in argon atmosphere, only a small quantity of Al₂O₃ is formed. In addition, the nano AlN becomes a crystallization nucleus and promotes the crystallization of α -SiO₂, β -SiO₂, and tridymite during the sintering process, and refine the microstructure of the crystal phase. The researchers involved further stated that the addition of nano AlN to the glass matrix can increase the flexural strength and wear resistance, with the optimal amount for addition being 6 wt% [10, 11].

In this study, a borosilicate glass was chosen as the matrix of the VBD tools, and 0 to 60 vol% of nano AlN was added into the matrix, after which sintering in the atmosphere was conducted. The sintered specimens were examined using an X-ray diffraction analyzer (XRD), a Raman spectrometer, and a scanning electron

*Corresponding author:
Tel : +886-2-8662-5917
Fax: +886-2-8662-5919
E-mail: khlin@mail.tnu.edu.tw

microscope (SEM) with an energy dispersive spectrum analysis (EDS). The microstructure observation and the measurement of sintered density, matrix hardness, and grinding ratio (G-ratio) test of the sintered specimen were also executed. The effects of the added nano AlN on the microstructure and mechanical properties of the VBD tools were investigated. Finally, the optimal amount of nano AlN to add in VBD tools is suggested based on the analytical results.

Experimental Procedure

Table 1 shows the composition of the borosilicate glass (China Glaze, CT-1124). The average particle sizes of the borosilicate glass and synthetic diamond (GE, FM 30-40) were around 20.6 μm and 30.8 μm , respectively. The nano AlN (Bojun, WU-AlN-001, density 0.15 g/cm^3) used in this study with a mean size around 50 nm. The synthetic diamond grits, borosilicate glass powder, and nano AlN, whose SEM micrographs

Table 1. Composition of borosilicate glass powder.

SiO ₂	B ₂ O ₃	Na ₂ O	CaO	ZnO
>40.0%	10.0-40.0%	3.0-10.0%	3.0-10.0%	3.0-10.0%
Al ₂ O ₃	K ₂ O	MgO	BaO	Li ₂ O
3.0-10.0%	0.1-3.0%	0.1-3.0%	0.1-3.0%	0.1-3.0%

are shown in Fig. 1. The specimens had a 1:3:1 volume proportion of diamond grits, glass powder, and paraffin wax. The designations and compositions of the specimens investigated in this study are shown in Table 2, with the added amounts of nano AlN ranging from 0 to 60 vol%.

The diamond grits and glass powder were mixed and blended in a plastic jar for 12 h in the presence of heptane and paraffin wax, using zirconia balls. The powder slurry was then dried at 60 °C for 90 min and the granules were sieved through a screen of 100 mesh. Nano AlN was subsequently added and mixed with the dried granules according to the experimental condition.

Table 2. Compositions of specimens investigated in this study.

Specimens	Diamond grit (vol%)	Glass powder (vol%)	Paraffin Wax (vol%)	AlN (vol%)	AlN (wt%)
0A	20	60	20	0	0
5A	19	57	19	5	0.4
10A	18	54	18	10	0.8
20A	16	48	16	20	1.7
30A	14	42	14	30	2.8
40A	12	36	12	40	4.3
50A	10	30	10	50	6.4
60A	8	24	8	60	9.3

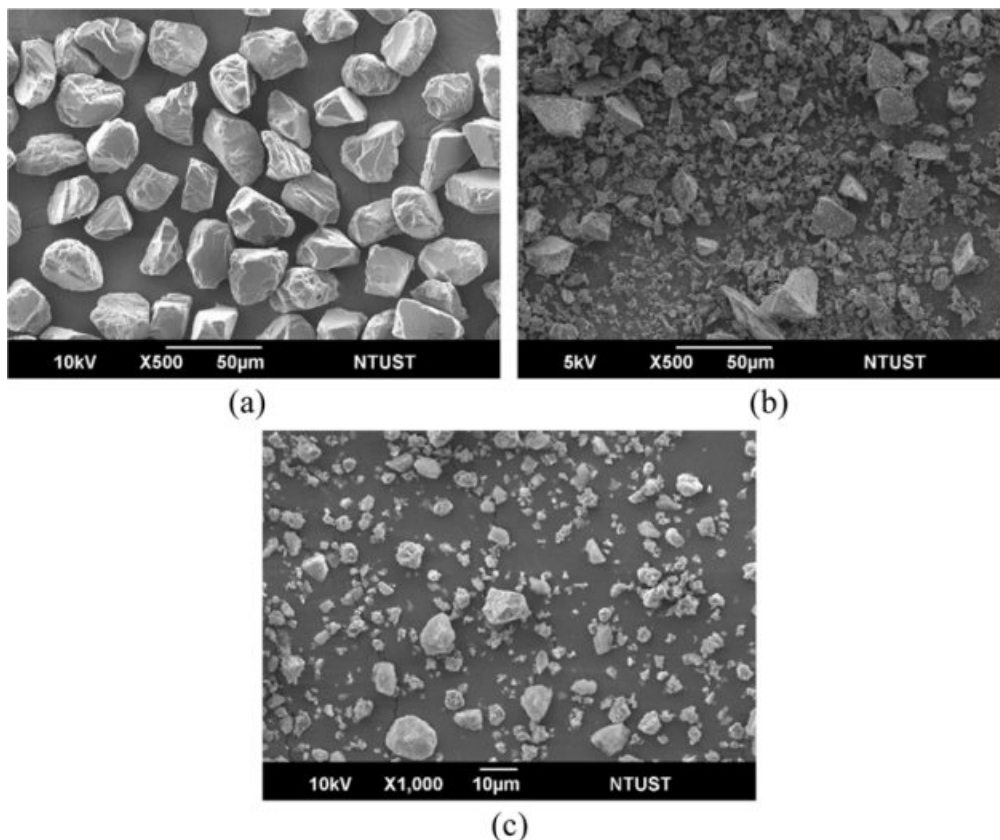


Fig. 1. SEM micrographs of the: (a) diamond grits, (b) glass powder, and (c) nano AlN used in this study.

mm in diameter and 3 mm in height, were die-pressed with a pressure of 30 MPa. The thermal profile was composed of heating at 5 °C/min to 250 °C, held for 30 min to burn off the paraffin, and then 3 °C/min to 600 °C, held for 60 min. This profile was followed by heating at 1 °C/min to 690 °C, held for 90 min. All of the specimens were then furnace-cooled. A constant air flow was maintained in order to clear the tube furnace until the temperature reached 500 °C, after which the specimens were sintered in the atmosphere.

A thermogravimetric analyzer (TGA, TA Instrument Q500) and a differential scanning calorimetry (DSC, Netzsch Instrument 404 F3) applied a heating rate of 5 °C/min from 25 °C to 900 °C were carried out for thermal analyses of the diamond grits and glass powder, respectively. The XRD (Shimadzu, XRD-6000) with Cu Ka radiation at an acceleration voltage of 30 kV and current of 30 mA, and diffraction angles of 20° to 100° was carried out for examined the sintered specimens. A Raman spectrometer (Lambda Solution, P2) was used to investigate the possible degradation of diamond grits at high temperatures. The wavelength of the excitation laser was 780 nm. A SEM (JEOL, JSM-6390LV) with a working voltage 30 kV was used for examined the microstructure of sintered specimens and G-ratio test specimens. In addition, this study also analyzes the radial shrinkage percentages, sintered densities, matrix hardness, and G-ratios of the sintered specimens. The surface roughness of the workpieces after G-ratio tests was recorded by a surface roughness measuring instrument (Kosaka Laboratory Ltd, SEF-3500).

Results and Discussion

Thermal analysis

The diamond powder used in this study was subjected to thermogravimetric analysis under an atmospheric environment. The results showed a rapid weight loss of the diamonds between 620 °C and 720 °C, with the weight loss being close to 90 wt% at the temperature of 720 °C (Fig. 2(a)). The DSC analyze of glass powder and paraffin wax was observed an endothermic peak at 203 °C, which indicating the volatilization temperature of the paraffin, and also revealed that glass transition temperature (T_g) was approximately 716 °C (Fig. 2(b)). In addition, the glass softening temperature offered by the glass powder manufacturer was approximately 640 °C.

Raman spectroscopy analysis

The Raman spectra of all the sintered specimens were shown in Fig. 3. A sharp peak at 1330.4 cm⁻¹ can be observed, which belongs to the crystalline diamond C-C bond D-band signal [16-19]. It is notable that the intensity of the D-band signal varies according to the amount of nano AlN that was added. The 10A and 20A specimens had the most intense D-band signals, which

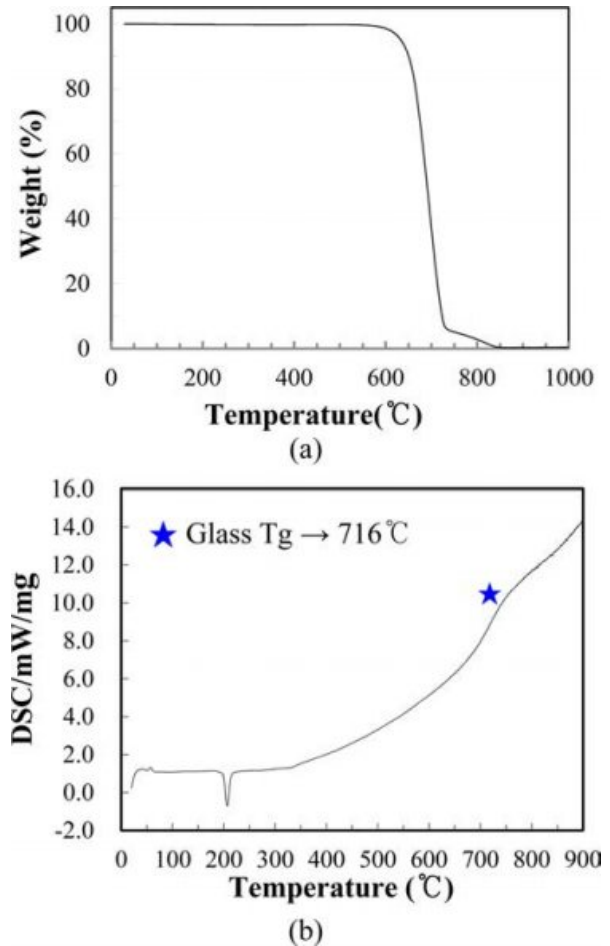


Fig. 2. Thermal analysis: (a) TGA curve of the diamond powder, and (b) DSC curve of the glass powder.

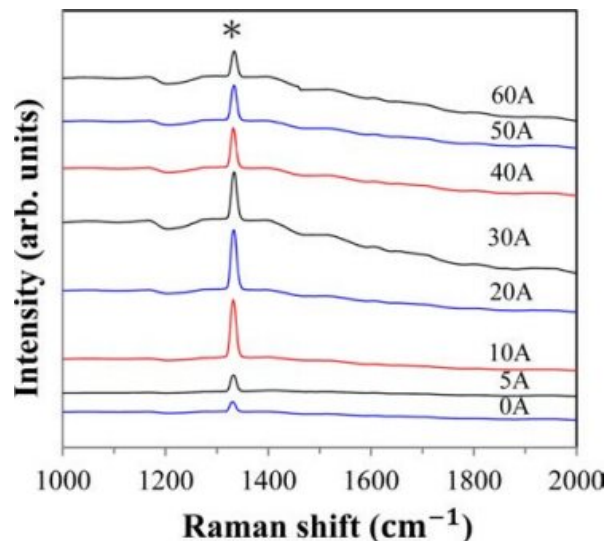


Fig. 3. Raman spectra of all sintered specimens.

indicated that the amounts of nano AlN added to these specimens were the most appropriate for protecting the crystal structure of the diamond during sintering.

However, the D-band signal intensity gradually

decreased when the amount of nano AlN added over 20 vol%, and resulting in diamond crystal with lower quality and composition. Moreover, no obvious G-band signals belonging to the graphite were observed at the range of 1550 cm^{-1} to 1600 cm^{-1} . As such, it was concluded that the sintering parameters of a sintering temperature of $690\text{ }^{\circ}\text{C}$ and isothermal holding for 90 min used in this study are appropriate for the fabrication of VBD tools.

XRD analysis

Fig. 4 displays the XRD patterns of the sintered specimens 0A, 10A, 20A, 40A, and 60A. Three obvious diffraction peaks were observed, the 2θ angles were 44.0° , 75.3° , and 91.5° , respectively, which correspond to the 2θ angles of the (111), (220), and (311) planes of diamond crystal (JCPDS 65-0537). It is noteworthy that the specimens added with higher percentages of nano AlN exhibited the stronger diffraction peaks of diamond crystal. In addition, the 40A and 60A specimens also exhibited the diffraction peaks of AlN, the 2θ angles of which were 33.1° , 35.8° , 37.9° , 49.8° , 59.2° , and 71.3° , respectively, which corresponded to 2θ angles of the (100), (002), (101), (102), (110) and (112) planes of aluminum nitride (JCPDS 89-3446). However, for the specimen to which 10 vol% AlN was added, no obvious diffraction peaks of AlN were observed.

As can be seen in Fig. 4, not only the diffraction peaks of diamond and AlN but also those of the Al_2O_3 phase (JCPDS 81-1667) were observed. In addition, two tiny diffraction peaks of SiO_2 phase (JCPDS 89-7499) were also observed between the two theta values of 20° and 30° . As noted above, previous studies have reported that nano AlN is easily oxidized and decomposed into Al_2O_3 and NO_2 when sintering in the air, as well as nano AlN sintered in argon becomes a crystallization nucleus and promotes the crystallization of $\alpha\text{-SiO}_2$, $\beta\text{-SiO}_2$, and tridymite during the sintering process [10-

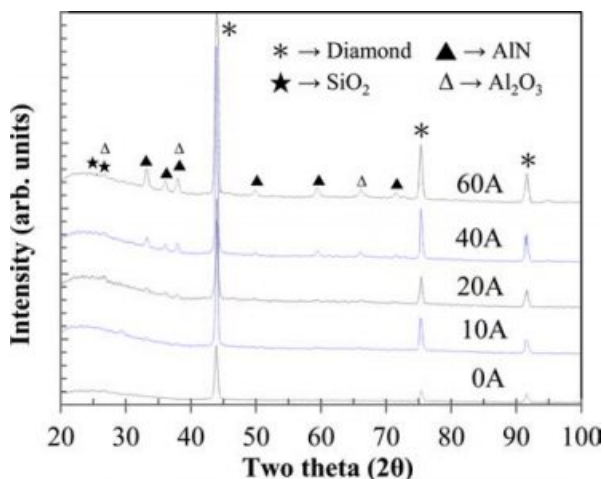


Fig. 4. XRD patterns of five sintered specimens.

11]. However, only the Al_2O_3 phase was clearly observed in our study. The sintering temperature used in this study was only $690\text{ }^{\circ}\text{C}$, maybe the lower sintering temperature have resulted in less phase formation of $\alpha\text{-SiO}_2$ and $\beta\text{-SiO}_2$, such that those could not be detected clearly in the XRD patterns [20, 21].

Microstructure analysis

Fig. 5 displays the SEM micrographs of the sintered specimens 0A, 5A, 10A, and 20A, respectively. The diamond grits had a good wetting and intimately covered by the vitrified bond. The number of pore in the vitrified matrix had a little bit increased when the amount of AlN added was increased.

Fig. 6(a) displays the SEM micrograph of the sintered specimen 30A. Compared with the specimen 20A, specimen 30A exhibited more pores, and the vitrified matrix gradually formed a loose structure. Consequently, the wetting between the diamond and vitrified bond was deteriorated, and resulted in inadequate bonding force between the diamond grits and the vitrified matrix. Fig. 6(b) displays the SEM micrograph of the sintered specimen 40A. The proportion of pore in the vitrified matrix was higher than that of the specimen 30A. In addition, some of irregularly shaped white particles with sizes around several μm were observed on the surface of the vitrified matrix.

Fig. 6(c) displays the SEM image of the sintered specimen 50A. The porosity in the vitrified matrix was even higher than that in the specimen 40A, the wetting between the diamond grits and the vitrified matrix were even greater deterioration, and thus the diamond grits were not fixed strongly. In addition, at the vitrified matrix surface more irregular shaped white particles were observed. Fig. 6(d) displays the SEM micrograph of the sintered specimen 60A. The large pores were observed around the diamond grits, and the bonding between the diamond grit and vitrified matrix was severely inadequate. Furthermore, much more of irregularly shaped white particles were observed in the matrix surface.

Fig. 7(a) shows a high-magnification SEM image of sintered specimen 60A. The arrow in Fig. 7(a) indicates an irregularly shaped particle with a size around several μm . According to the energy dispersive spectrum (EDS) analysis, the components of the white particle included the following: Si (22.1 at%), O (10.6 at%), Na (17.1 at%), B (6.1 at%), Zn (3.6 at%), Al (20.6 at%), N (10.8 at%), etc. The analysis results indicated that the irregularly shaped particle was a mixture of the glass and aluminum nitride or alumina.

The SEM images of Fig. 6(b) to 6(d) show that, with an increase of nano AlN, the numbers of irregularly shaped particles on the matrix surfaces were increased. Such a variation was due to that sintering was proceeded in the atmospheric environment, the nano AlN reacts with oxygen easily, consequently, the nano AlN was

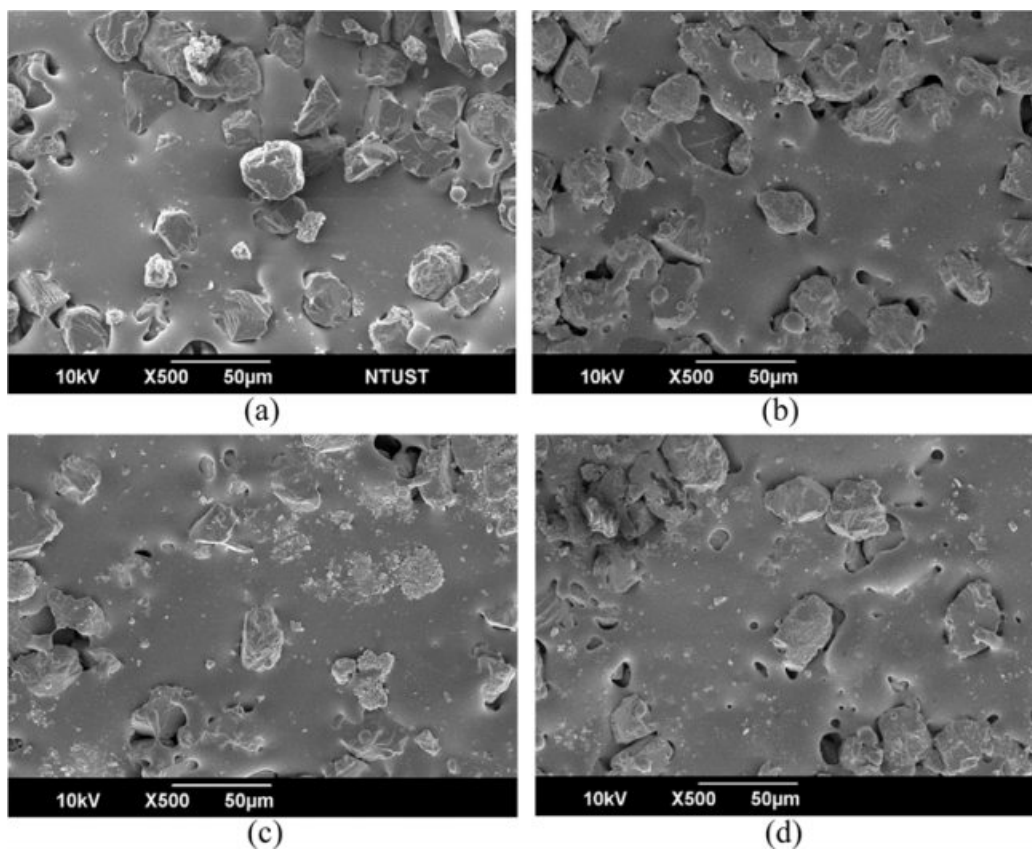


Fig. 5. SEM images of specimens: (a) 0A, (b) 5A, (c) 10A, and (d) 20A.

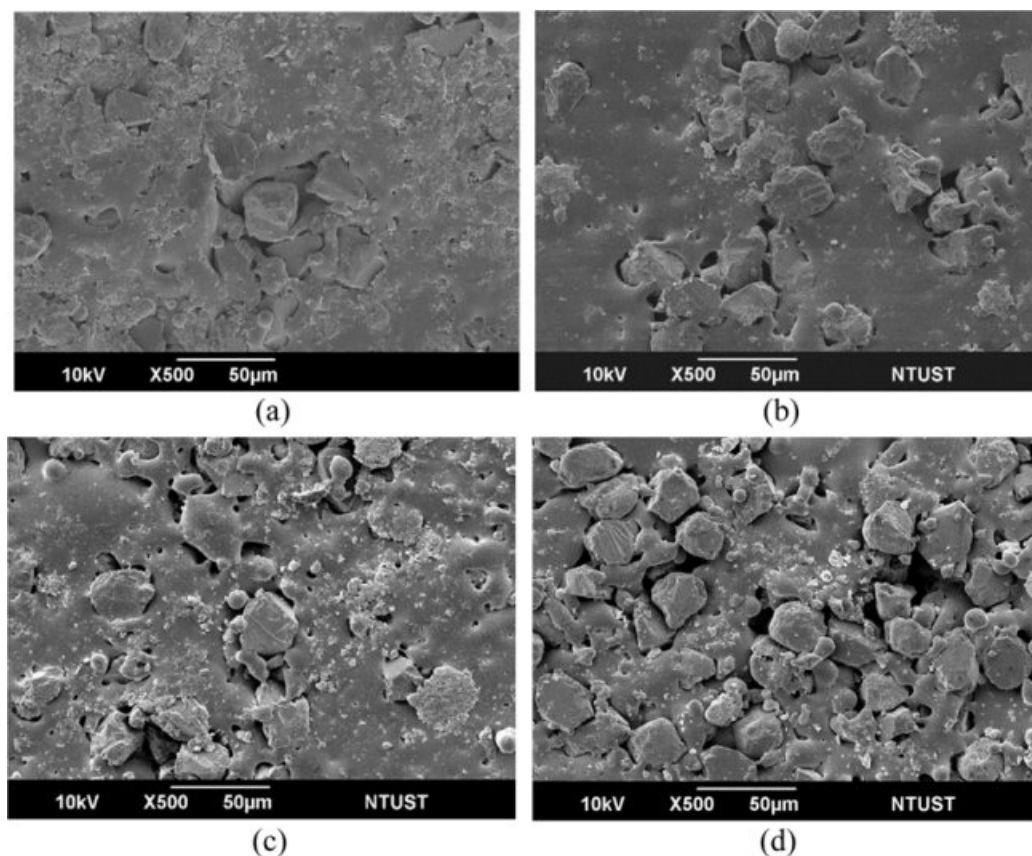


Fig. 6. SEM images of specimens: (a) 30A, (b) 40A, (c) 50A, and (d) 60A.

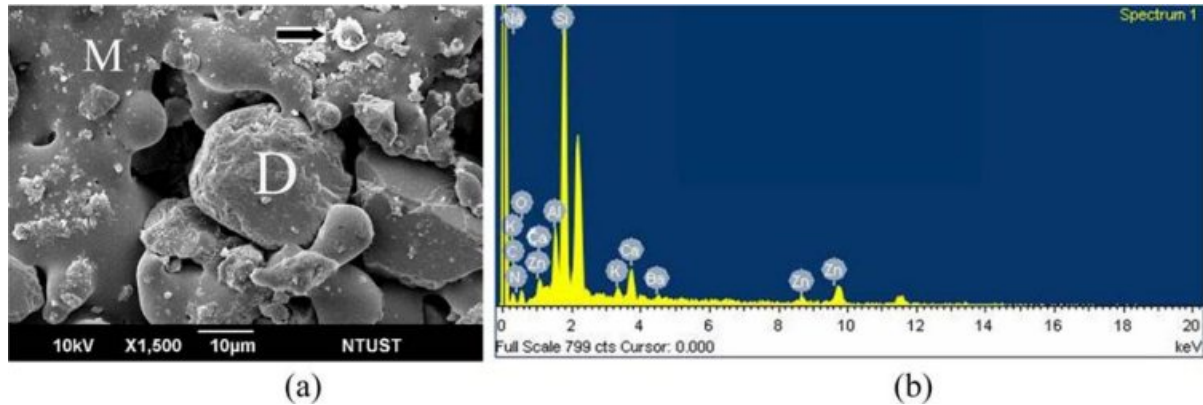


Fig. 7. Sintered specimen 60A: (a) SEM image (M: matrix, D: diamond), (b) EDS spectrum.

decomposed into alumina and nitrogen dioxide [10, 11], or the nano AlN was transformed into AlOH and Al₂O₃ accompanied by NH₃ gas [22-24]. Clearly, increased the added amount of nano AlN, the proportion of gas generated from the specimen was increased also. The gas resulted in the eruption of the mixture which contains the glass and AlN or Al₂O₃ from the inside of the matrix, thus greater the porosity around the diamond.

Shrinkage percentage and sintered density

The measurement of radial shrinkage percentages of the sintered specimens were calculated by averaging five tests. The sintered density of the specimen was analyzed using the Archimedes method, each sintered specimen being measured three times. Fig. 8 presents the radial shrinkage percentages and sintered densities of all the sintered specimens.

The radial shrinkage percentage and sintered density of specimen 0A were 14.20% and 2.43 g/cm³, respectively. The radial shrinkage percentage of specimen 5A (14.27%) was higher than that of specimen 0A by 0.5%, and the sintered density was increased by 0.8%. The radial shrinkage percentage of specimen 10A (15.30%) was higher than that of specimen 0A by

7.7%, and the sintered density was increased by 3.3%. However, it can be observed that the radial shrinkage percentage and sintered density gradually decreased when the amount of nano AlN added was higher than 20 vol%. The decrease in the radial shrinkage percentage and sintered density were especially evident for the specimens 40A to 60A. Such a variation was believed to arise from the expansion of the vitrified matrix, as shown in SEM images previously. The vitrified matrix exhibited high porosity due to the matrix expansion when the amount of nano AlN added was higher than 20 vol%. According to the above observations, it can be concluded that the optimal amount of nano AlN to add should be 10 vol%, because the 10A specimen possessing the best radial shrinkage percentage and sintered density.

Hardness test

The hardness value of the vitrified matrix was measured using a micro Vickers hardness (mHV) tester (Makazawa, HM-221) with a load of 19.6N and a holding time of 20 seconds. Each sintered specimen was measured five times and then averaged. Fig. 9 presents the average hardness values of the vitrified

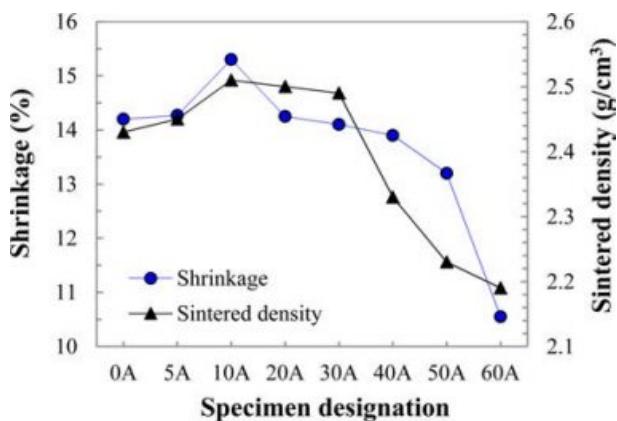


Fig. 8. Radial shrinkage percentages and sintered densities of all sintered specimens.

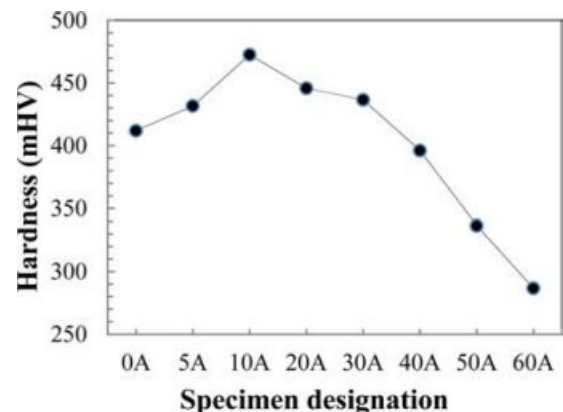


Fig. 9. Hardness values of the vitrified matrix of all sintered specimens.

matrix of all sintered specimens. The hardness value of specimen 5A (mHV 431.7) was higher than that of specimen 0A (mHV 411.9) by 4.8%. The hardness value of specimen 10A (mHV 472.5) was higher than that of specimen 0A by 14.7%. It can be concluded that when the added amounts of nano AlN were lower than 10 vol%, the hardness increased as the added amount increased.

However, for the amounts of nano AlN was added higher than 10 vol%, the hardness decreased as the added amount increased. The hardness value of specimen 20A (mHV 445.8) was lower than that of specimen 10A by 5.6%. The hardness value of specimen 30A (mHV 436.6) was lower than that of specimen 10A by 7.6%. The specimen 60A had the lowest hardness value (mHV 286.7). This observation indicates that the addition of a suitable amount of nano AlN contributed to the hardness of the vitrified matrix. In this study, the optimal amount of added nano AlN was 10 vol%. The SEM images shown previously also confirm when the quantity of nano AlN added was over 20 vol%, the matrix expansion will occur, and thus the hardness will be decreased.

Grinding ratio tests

G-ratio test of the VBD tool was performed using a high speed lathe at a rotation speed of 1800 rpm. A disc shape sintered specimen (VBD tool) with an outer diameter of 30 mm and a thickness of 3 mm was used as the cutting tool. A tungsten carbide rod with an outer diameter of 4.5 mm (WC87%-Co13%, density 14.17 g/cm³) was used as the workpiece for the G-ratio test. The grinding length of the tungsten carbide rod was set as 10 mm. The cutting depth of the tungsten carbide rod was 0.01mm/pass, the lateral feeding rate of tungsten carbide rod to the VBD tool was 0.0125 mm/sec, and water was used as the coolant. The weight loss of the VBD tool and tungsten carbide rod were recorded after the given grinding test. The definition of G-ratio is (volume loss of tungsten carbide rod) / (volume loss of VBD tool).

The G-ratios of the sintered specimens 0A, 5A, 10A, 20A, 30A, and 40A were 22.7, 23.2, 24.1, 23.6, 23.0, and 22.5, respectively (Fig. 10). The G-ratio of specimen 5A (23.2) was higher than that of specimen 0A (22.7) by 2.2%. The G-ratio of specimen 10A (24.1) was higher than that of specimen 0A by 6.2%. The G-ratio of specimen 20A (23.6) was higher than that of specimen 0A by approximately 4.0%. It was found the G-ratios of VBD tool gradually decreased when the amount of nano AlN added was over 10 vol%, due to the microstructure variation and vitrified matrix hardness value decreased.

Fig. 11 displays the SEM micrographs of sintered specimens 5A, 10A, 30A, and 40A after the G-ratio tests. Fig. 11(a) shows the wetting between the vitrified matrix and diamond grit was appropriate, but several

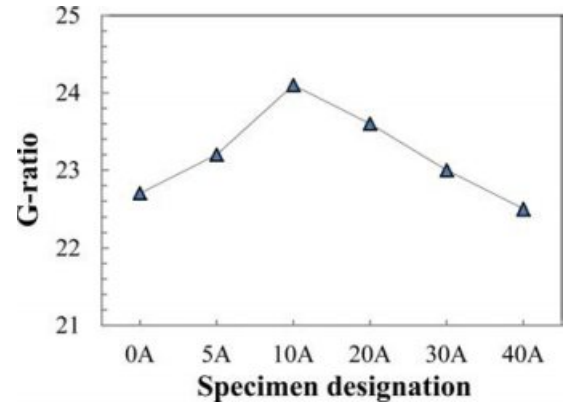


Fig. 10. Grinding ratio values of six sintered specimens.

pores with sizes approximately 5 μm to 10 μm were present around the diamond grit. Compared with the specimen 5A, the specimen 10A had a fewer, and a smaller size of pores around the diamond grit (Fig. 11(b)). The size of pores around the diamond gradually increased when the amount of nano AlN added exceeded than 20 vol%. Fig. 11(c) and 11(d) show the SEM images of specimens 30A and 40A, respectively. Pores with sizes over 10 μm were observed, and these pores resulted in the diamond grit and vitrified matrix unable bonding strongly, which in turn caused the diamond grit to be pulled out from the vitrified matrix before becoming worn. Therefore, the specimens 30A and 40A had relatively a lower G-ratio. The appropriate porosity around the diamond grit assists in heat dissipation and preserves the cutting fluid of the VBD tools. However, too much porosity and large pores decrease the bonding strength between the diamond and vitrified matrix, consequently result in VBD tools with a lower G-ratio, and inferior the workpiece surface roughness.

A three dimension surface roughness analysis apparatus (Kosaka Laboratory, SEF-3500) was used to detect the surface roughness of the workpiece after the G-ratio test. The center line average roughness (Ra) method was employed and a three dimension scanning image of the workpieces was taken. Fig. 12 shows the surface roughness values of six workpieces after the G-ratio tests were 0.66 μm , 0.39 μm , 0.35 μm , 0.37 μm , 0.56 μm , and 0.65 μm , respectively. In this work, specimen 10A had the highest G-ratio (24.1) and workpiece possess with the best surface roughness (Ra, 0.35 μm). The specimens 40A had the lowest G-ratio (22.5) and workpiece possess with the worst surface roughness (Ra, 0.65 μm).

Fig. 13 displays the three dimension surface morphologies of the workpieces that ground by VBD tools 5A, 10A, and 20A, respectively. The workpiece ground by VBD tools 10A had the best surface morphology (Fig. 13(b)), and the workpieces ground by VBD tools 5A and 20A had slightly poorer surface morphologies (Fig. 13(a))

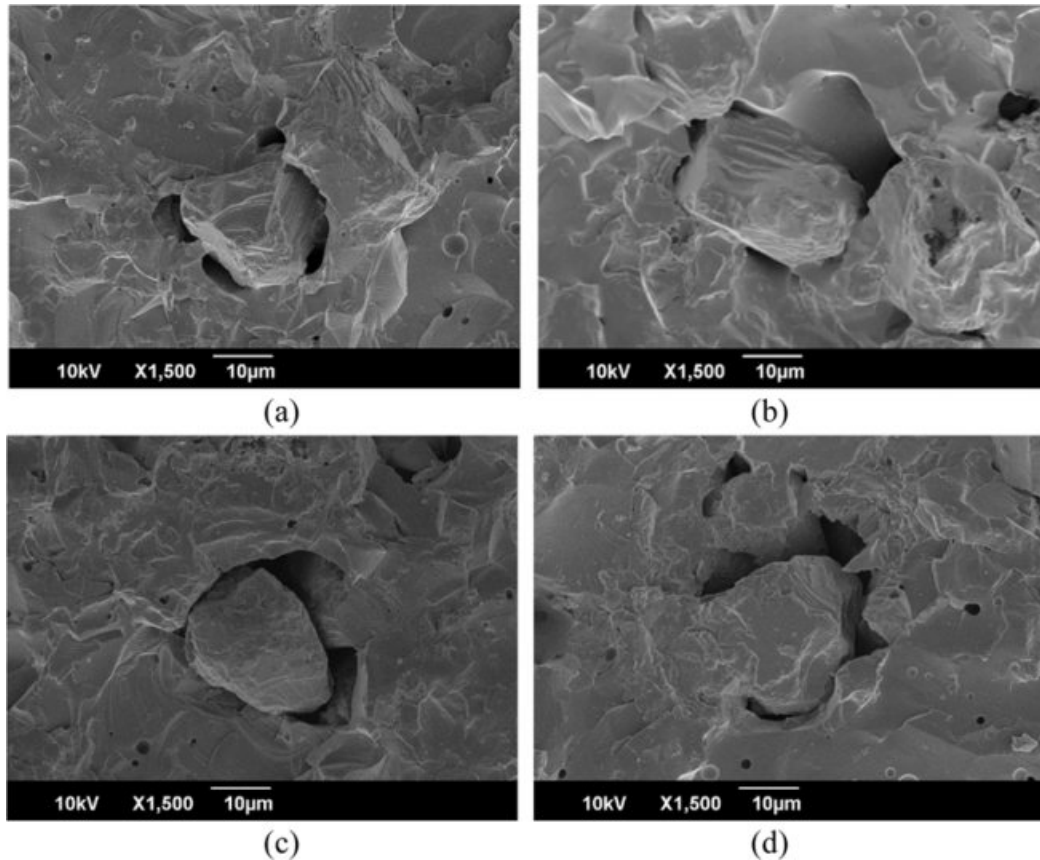


Fig. 11. SEM micrographs after G-ratio tests for specimens (a) 5A, (b) 10A, (c) 30A, and (d) 40A.

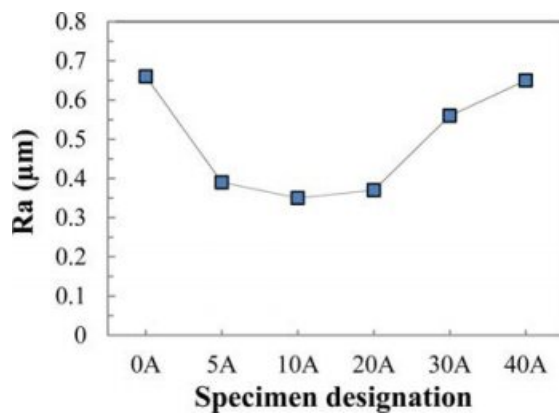


Fig. 12. The surface roughness values of workpieces after G-ratio tests.

and Fig. 13(c)). As described previously, when the amount of nano AlN added exceeded than 20 vol%, there were a higher proportion of pores exist in the vitrified matrix, thus the bonding force of the diamond grits were degraded. A poor bonding between the diamond grits and vitrified matrix also increased the workpiece surface roughness. However, the over tight bonding between the diamond and vitrified matrix also prevents the diamond grit from being pulled out of the matrix even when it becomes worn, and thus results in the

workpiece's surface roughness increased. Not only a proper G-ratio but also a good workpiece surface roughness is required for the outstanding VBD tool. Therefore, the bonding force between the diamond and matrix should be adjusted as necessary, so that the diamond grit can be pulled out from the vitrified bond when it becomes blunt. Moreover, an appropriate porosity and brittleness of the matrix allows a VBD tool to maintain its sharpness and also achieves a better workpiece surface roughness.

Conclusions

The Raman spectra analysis indicated added of 10 vol% to 20 vol% nano AlN into the VBD tool assisted to protect the diamond crystal structure during the sintering process. The XRD analysis results revealed the obvious diffraction patterns of the diamond crystal in all of the sintered specimens. However, only the 40A and 60A sintered specimens exhibited the weak diffraction patterns of AlN, Al₂O₃, and SiO₂ phases, possibly due to the lower sintering temperature of 690 °C used in this study. The SEM image indicated the VBD tool added of 10 vol% AlN had an optimal microstructure; it also had an appropriate grinding ratio and a good workpiece surface roughness. As the added amount of nano AlN exceeded than 20 vol%, it resulted

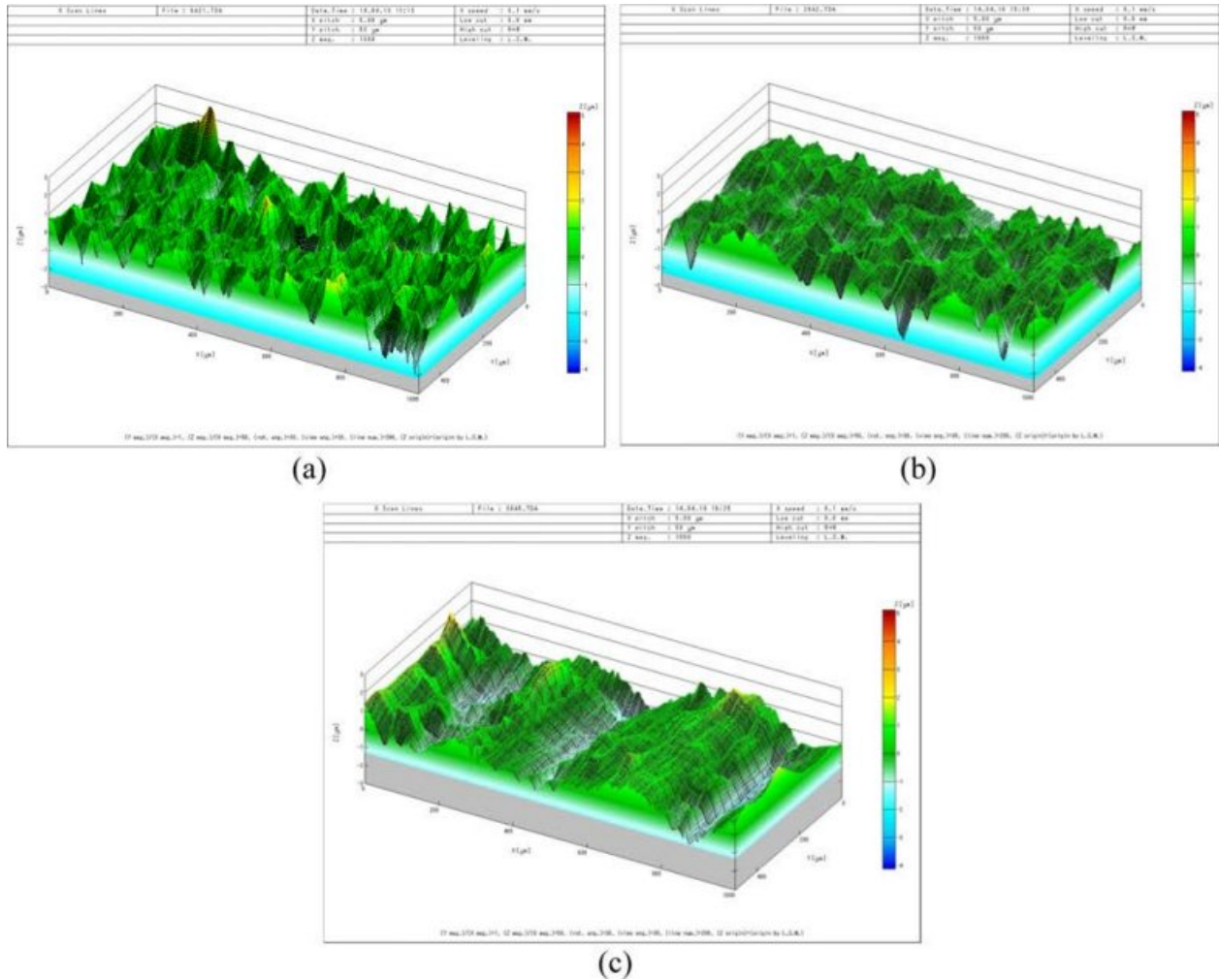


Fig. 13. Three dimension surface morphologies of the workpieces ground by specimens (a) 5A, (b) 10A, and (c) 20A.

in expansion of the vitrified matrix due to the gas formation. The bonding strength between the diamond grit and matrix was descended; so that G-ratio of the VBD tool was decreased. The specimen 10A had the optimal workpiece surface roughness, followed by specimen 20A. In this study, the VBD tool added with 10 vol% (0.8 wt%) nano AlN had the best G-ratio and workpiece surface roughness.

Acknowledgment

We thank the Ministry of Science and Technology for providing financial support for this study (study plan MOST 103-2221-E-236-002).

References

1. K.H. Lin, S.F. Peng, and S.T. Lin, *Int. J. Refract. Met. Hard Mater.* 25[1] (2007) 25-31.
2. T.K. Chuang, Y.T. Tsai, and K.H. Lin, *Int. J. Refract. Met. Hard Mater.* 74 (2018) 107-113.
3. Y.X. Sun, Y.T. Tsai, and K.H. Lin, *Mater. Des.* 80 (2015) 89-98.
4. S. Ogawa and T. Okamoto, *Bull. Jpn. Soc. Prec. Eng.* 20[4] (1986) 264-271.
5. T. Tanaka, N. Ikawa, N. Ueno, and S. Okada, *Bull. Jpn. Soc. Prec. Eng.* 19[3] (1985) 221-222.
6. Y. Kuroshima, Y. Kondo, and S. Okada, *J. Ceram. Soc. Jpn.* 93[9] (1985) 587-589.
7. X.F. Liu and Y.Z. Li, *Int. J. Refract. Met. Hard Mater.* 21[3-4] (2003) 119-123.
8. H.W. Choi, S.J. Kim, H. Yang, Y.S. Yang, Y.H. Rim, and C.R. Cho, *J. Ceram. Process. Res.* 20[1] (2019) 63-68.
9. X.H. Zhang, Y.H. Wang, J.B. Zang, and X.Z. Cheng, *Int. J. Refract. Met. Hard Mater.* 29[4] (2011) 495-498.
10. Y. Shang, Y.G. Hou, G.Y. Qiao, W.J. Zou, F.R. Xiao, and B. Liao, *Nonferr. Metal. Soc. China.* 19 (2009) s706-s710.
11. Y.G. Hou, G.Y. Qiao, Y. Shang, W.J. Zou, F.R. Xiao, and B. Liao, *Composites: Part B Eng.* 42[4] (2011) 756-762.
12. N. Zhang, T.T. Fu, F.Y. Yang, H.M. Kan, X.Y. Wang, H.B. Long, and L.Y. Wang, *J. Ceram. Process. Res.* 15[2] (2014) 93-96.
13. X.H. Zhang, Y.H. Wang, J.B. Zang, X.Z. Cheng, X.P. Xu, and J. Lu, *J. Eur. Ceram. Soc.* 31[10] (2011) 1897-1903.
14. N. Yan, D.P. Zhao, L. Wang, Q. Zou, Y.Y. Xi, X.P. Guo, B. Wang, Z.L. Wang, L.P. Wang, W.J. Dai, M.Z. Wang, and Y.C. Zhao, *Int. J. Refract. Met. Hard Mater.* 43 (2014) 212-

- 215.
15. X.H. Zhang, Y.H. Wang, J. Lu, J.B. Zang, J.H. Zhang, and E.B. Ge, *Int. J. Refract. Met. Hard Mater.* 28[2] (2010) 260-264.
 16. J. Wagner, M. Ramsteiner, Ch. Wild, and P. Koidl, *Phys. Rev. B.* 40 (1989) 1817-1823.
 17. J.J. Wang, H. Yan, Y.J. Deng, H.D. Li, Y.F. Zhang, F. Zhang, Z. Xia, Q. Gao, W. Du, H. Zhou, and Y. Zou, *Solid State Commun.* 115[4] (2000) 173-177.
 18. A.C. Ferrari, *Diam. Relat. Mater.* 11[3-6] (2002) 1053-1061.
 19. S. Prawer, K.W. Nugent, D.N. Jamieson, J.O. Orwa, L.A. Bursill, and J.L. Peng, *Chem. Phys. Lett.* 332[1-2] (2000) 93-97.
 20. K.S. Kim, S.H. Shim, S. Kim, and S. O. Yoon, *J. Ceram. Process. Res.* 11[1] (2010) 35-39.
 21. C.L. Liao, K.H. Lin, and S.T. Lin, *J. Ceram. Process. Res.* 9[6] (2008) 562-568.
 22. R. Metselaar, R. Reenis, M. Chen, H. Gorter, and H.T. Hintzen, *J. Eur. Ceram. Soc.* 15[11] (1995) 1079-1085.
 23. Y.H. Zhang, *Mater. Res. Bull.* 37[15] (2002) 2393-2400.
 24. D. Hotza, O. Sahling, and P. Greil, *J. Mater. Sci.* 30[1] (1995) 127-132.